Electronic Supplementary Information

The Design of MOF-Based Nano-Trap for the Efficient Separation of Propane and Propylene

*Hua Zhu,[a,1] Yue Wang,[a,1] Xin Wang,[a] Zi-Wen Fan,[a] Hui-Fang Wang,[*a] Zheng Niu,[*a] Jian-Ping Lang[*a,b]*

[a] *College of Chemistry, Chemical Engineering and Materials Science, Soochow University, Suzhou, Jiangsu, 215127.*

[b] *State Key Laboratory of Organometallic Chemistry, Shanghai Institute of Organic Chemistry, Chinese Academy of Sciences, Shanghai 200032.*

[1]*Correspondence: These authors contribute equally to this work.*

zhengniu@suda.edu.cn;

wanghf@suda.edu.cn;

jplang@suda.edu.cn;

Table of Contents

Experimental Procedures

All of the chemicals except adamantanetetracarboxylic acid were obtained from commercial sources and, unless otherwise noted, were used as received without further purification. The gases including propylene, propane gas used in this work are high purity gases.

Synthesis of *1, 3, 5, 7*-adamantanetetracarboxylic acid (H_4ATC)

The synthesis of *1, 3, 5, 7*-adamantanetetracarboxylic is similar to the literature[S1] but with slight modifications.

Tetramethyl 2,6-dioxo-bicyclo[1.3.3]-nonane-1,3,5,7-tetracarboxylate (**a**). A mixture of dimethyl malonate (66.0 g, 0.51 mol) and aqueous formaldehyde (40 wt%, 30.0 g, 0.39 mol) was cooled to 0 °C. Diethyl amine (2.4 g, 0.03 mol) was added to the dropping funnel, then added to the reaction solution dropwise. After 10 min, the viscous colorless solution was diluted by sufficient methanol (4.0 mL) to give a clear solution. After 12 h at 0 °C, 24 h at 25 °C, 48 h at 40 °C, and then stop stirring and cooling to 0 °C. After 1 h, the aqueous layer was removed. The organic residue was washed successively with 2 N sulfuric acid and ice water for three times. The residual viscous liquid was heated under vacuum [100 °C (1 mmHg)] overnight to remove unreacted malonate. The resulting viscous oil was treated with 40 mL 3 M sodium methoxide methanol solution, prepared from sodium methoxide (19.44 g, 0.36 mol) in MeOH (120.0 mL), and then refluxed for 4 h at 100 °C. MeOH was removed in vacuo to afford a residue, which was treated with ice-cold water (100.0 mL). After that, 150 mL 4 M HCl was added into the aqueous methanol solution to obtain the white solid, which was filtered, washed thoroughly with excess water, and finally recrystallized from boiling MeOH to afford (75%) a as light-rose tetramethyl 2,6-dioxobicyclo[1.3.3]-nonane-1,3,5,7- (**a**) as the tetracarboxylate colored prismatic crystals: 10.0 g; ^{1}H NMR δ 2.32 (s, 2 H), 2.87 (s, 4 H), 3.76-3.78 (br s, 14 H); IR (KBr) 3400, 3000, 1740, 1622 cm^{-1}.

Tetramethyl 2,6-dioxoadamantane-1,3,5,7-tetracarboxylate (**b**). Dissolving the tetramethyl 2,6-dioxobicyclo[1.3.3]-nonane-1,3,5,7-tetracarboxylate (**a**) (2.5 g, 0.01 mol) into 5 mL 3 M sodium methoxide methanol solution, prepared from sodium methoxide (0.81 g, 0.015 mol) in MeOH (5 mL), then adding 4 mL CH_2Br_2 into the mixture methanol solution. The clean solution was put into 20 mL bomb steel and then heated at 130 °C overnight. After cooling 4 h at room temperature, the resultant crystallized solid was filtered and washed with MeOH and then a copious amount of water. After drying, the solid was recrystallized [dioxane-MeOH (1:2, volume ratio)] to give (30%) tetraester **b** 1.6 g; ^{1}H NMR (DMSO-d_6): δ 2.89 (s, 8 H), 3.79 (s, 12 H); IR (KBr): 1734, 1710, 3000, 2850 cm^{-1}.

1,3,5,7-adamantanetetracarboxylic acid (**c**). A mixture of **b** (1.0 g), hydrazine hydrate (85 wt%; 6.0 mL), and a 5 mL 3 M sodium methoxide methanol solution, prepared from sodium methoxide (0.81 g, 0.015 mol) in MeOH (5 mL), was heated slowly in a steel bomb. When the temperature rose to 200 °C, the

gaseous products were slowly and carefully removed. Heating was continued until the temperature reached 240 °C, and then the temperature was maintained for 8 h. After cooling, the dry reaction product was dissolved in water (25.0 mL), treated with charcoal, warmed, and filtered. The pale yellow filtrate was concentrated (10.0 mL) in vacuo and acidified with HCl (pH 1-2) to give (90% yield) **c** as colorless crystals: 0.3 g; ^{1}H NMR (DMSO-d_6): δ 2.6 (bs, 12 H); IR (KBr): 3105 (broad), 1709, 1450, 1398, 1194 cm^{-1}.

Synthesis of $[Cu_2(ATC)(H_2O)_2]\cdot 5H_2O$

The $[Cu_2(ATC)(H_2O)_2]\cdot 5H_2O$ was synthesized according to the method from literature with slight modification.[S2] A mixture of H_4ATC (0.035 g, 0.11 mmol) and $Cu(NO_3)_2\cdot 2.5H_2O$ (0.077 g, 0.33 mmol) in 3 mL 1×10^{-3} M aqueous NaOH was heated to 100 °C to get the clear blue solution. The aqueous solution was then heated to 200 °C for 18 h to give green crystals of ATC-Cu along with tiny amounts of crystalline H_4ATC. The solid was filtered and then washed with hot water several times and then get the pure ATC-Cu crystal in 46% yield.

Gas adsorption measurement

Crystalline samples (80-100 mg) of anhydrous ATC-Cu were activated for low-pressure gas sorption analysis were transferred to a pre-weighed 6-mm large bulb glass sample cell. The sample was degassed at 190 °C under high vacuum (<5 μm Hg) for 16 h prior to sorption analysis on an ASAP 2020 Surface Area and Porosity Analyzer (Micromeritics), equipped with a turbo molecular vacuum pump, during which time a color change from blue to dark purple occurred. The low-pressure gas sorption isotherms were collected on an ASAP 2020 Surface Area and Porosity Analyzer (Micromeritics) after activation of ATC-Cu. The apparent surface areas of ATC-Cu were determined from the nitrogen adsorption isotherm collected at 77 K by applying the Brunauer-Emmett-Teller (BET) and Langmuir models.

Ideal Adsorbed Solution Theory

Dual-Langmuir-Freundlich isotherm model[S3] was adopted to fit the single-component loadings for C_3H_6 and C_3H_8 at 298 K, as is shown in following equations:

$$n(P) = \frac{n_{m1}b_1P^{\left(\frac{1}{t_1}\right)}}{1+b_1P^{\left(\frac{1}{t_1}\right)}} + \frac{n_{m2}b_2P^{\left(\frac{1}{t_2}\right)}}{1+b_2P^{\left(\frac{1}{t_2}\right)}}$$

In this equation, n is the amount adsorbed per mass of material (in mmol g^{-1}), P is the total pressure (in kPa) of the bulk gas at equilibrium with the adsorbed phase, n_{m1} and n_{m2} are the saturation uptakes (in mmol g^{-1}) for sites 1 and 2, b_1 and b_2 are the affinity coefficients (in kPa^{-1}) for sites 1 and 2, and t_1 and t_2 represent the deviations from the ideal homogeneous surface (unitless) for sites 1 and 2. The parameters that were obtained from the fitting are found in **Table S5**. Both isotherms were fitted with $R^2 > 0.999$. Next, the spreading pressure for adsorbates i and j can be calculated using the following equations:

$$\frac{\pi^{\circ}_i A}{RT} = \int_0^{P^{\circ}_i(\pi)} \frac{n_i(P)}{P} dP$$
$$\frac{\pi^{\circ}_j A}{RT} = \int_0^{P^{\circ}_j(\pi)} \frac{n_j(P)}{P} dP$$

In the above equations, A represents the specific surface area (assumed to be the same for all adsorbates), R is the ideal gas constant, T is the temperature, and $P^{\circ}_i(\pi)$ and $P^{\circ}_j(\pi)$ are the equilibrium gas phase pressures corresponding to the solution temperature and solution spreading pressure for the sorption of pure components i and j, respectively. Further, the following equations hold true for a two-component mixture according to IAST[S4]:

$$\pi^{\circ}_i = \pi^{\circ}_j$$

$$Py_i = P^{\circ}_i x_i$$

$$Py_i = P^{\circ}_i x_i$$

$$x_i + x_j = 1$$

$$y_i + y_j = 1$$

Here, x_i and x_j are the mole fractions of components i and j, respectively, in the adsorbed phase, and y_i and y_j are the mole fractions of components i and j, respectively, in the gas phase. The previous seven equations are seven independent equations with nine unknowns. In order to solve all of the unknowns, two quantities must be specified, particularly P and y_i. Utilization of the aforementioned equations yield the following equilibrium expression for adsorbates i and j:

$$\frac{y_i}{(1-y_i)} \int_0^{P^{\circ}_i(\pi)} \frac{n_i(P)}{P} dP = \int_0^{P^{\circ}_j(\pi)} \frac{n_j(P)}{P} dP$$

The above equation was solved for x_i using numerical analysis for a range of pressures at a specified y_i value. Finally, the selectivity for adsorbate i relative to adsorbate j was calculated using the following:

$$S_{i/j} = \frac{x_i y_j}{x_j y_i}$$

The total amount of gas adsorbed within the mixture can be calculated using the following equation:

$$n_{tot} = \frac{n^{\circ}_i(P^{\circ}_i) n^{\circ}_j(P^{\circ}_j)}{x_i n^{\circ}_j(P^{\circ}_j) + x_j n^{\circ}_i(P^{\circ}_i)}$$

where $n^{\circ}_i(P^{\circ}_i)$ and $n^{\circ}_j(P^{\circ}_j)$ are the amount adsorbed in the standard state at the equilibrium gas phase pressure for sorbates i and j, respectively. The actual amount adsorbed for each component within the mixture can be calculated using the following:

$$n_i = n_{tot} x_i$$

$$n_j = n_{tot} x_j$$

Isosteric Heat of Adsorption

The experimental isosteric heat of adsorption (Q_{st}) values for C_3H_6 and C_3H_8 in ATC-Cu were determined by first fitting the adsorption isotherms at 273 K and 298 K for the respective adsorbates to the DSLF equation (see Ideal Adsorbed Solution Theory section above)[S5] and subsequently applying the Clausius-Clapeyron method.[S6] The parameters that were obtained from the fitting of the C_3H_6 and C_3H_8 adsorption isotherms are found in **Table S5**. All isotherms were fitted with $R^2 > 0.999$.

The fitted parameters were used to calculate the Q_{st} values for a range of uptakes through the Clausius-Clapeyron equation, which is the following:

$$Q_{st} = -R\frac{\partial \ln P}{\partial\left(1/T\right)}$$

where T is the temperature (in K) and R is the ideal gas constant. The partial derivative term actually represents the slope of the plot of ln P vs. $1/T$ for a number of isotherms at different temperatures at various loadings. Therefore, the above Q_{st} equation can be simplified to:

$$Q_{st} = -mR$$

where m is the slope, which can be calculated by the following for two different temperatures and their corresponding pressures:

$$m = \frac{T_1 T_2}{T_1 - T_2}\ln\left(\frac{P_2}{P_1}\right)$$

where $P_2 > P_1$ and $T_2 > T_1$. The P_i values were back-calculated for a range of uptakes using the DSLF equation *via* an iterative technique (e.g., the Newton-Raphson method) [S6].

Modeling Studies

All the cluster calculations, including the geometry optimization and adsorption conformation, are all performed in the Gaussian 09.[S7] All periodic structural optimization and DOS analysis are calculated in VASP.

Cluster Calculation Details. The theoretical investigation was carried out using density functional theory (DFT) calculations employing the hybrid B3LYP functional empirically corrected to include a long-range dispersion term as proposed by Grimme[S8] and referred to hereafter as DFT-D3. 6-31G* basis set[S9] was used for metalloid atoms, and Lanl2dz basis set[S10-S12] was used for Cu. All calculations were performed with a development version of the Gaussian 09.[S7] For geometry optimization, the default convergence criteria were used. Equilibrium structures were used to compute the binding energy for each adsorbed molecule (CO_2, C_3H_6 and C_3H_8).

$$\Delta E_{ads} = E_{cluster/X} - E_{cluster} - E_X$$

$E_{cluster/X}$ represents the total energy when "X" molecules are adsorbed on cluster, $E_{cluster}$ means the energy of the Cu paddle-wheels, while E_X is the energy of the "X" molecule. The calculated ΔE values for adsorption energy of "X" molecule. **Table S2** show the optimized energy after adsorbing C_3H_6 and C_3H_8, respectively.

Traditional calculations require a massive amount of computing power to obtain precise adsorption configuration owing to the excessive number of atoms in the periodic structure of MOFs. Therefore, to simplify MOFs' periodic structure, the cluster model with the primary adsorption site can significantly save the computing power. The previous works indicated that the binding energy of C_3H_6 for open metal sites is obviously higher than ligands, hence simplifying the ligands and used cluster model with the primary adsorption site would approximately evaluate the C_3H_6 adsorption capability of the MOFs. A series of models with the different distances of opposite Cu paddle-wheels was constructed (the distance was donated as D, and $3.8 \leq D \leq 8.8$ Å). C_3H_6/C_3H_8 molecules were placed around clusters (cluster immobilization) at different distances for structural optimization. Based on their binding energies for adsorption of C_3H_6/C_3H_8 molecules, reasonable distances at which adjacent opposite Cu-paddle wheels can produce synergistic effects were obtained.

Thermodynamic parameters and nature of binding forces. Most interactions between gas molecules and MOFs, namely hydrogen bonding, electrostatic force, van der Waals force, which play a key role in the interactions. The thermodynamic parameters relying on the temperatures, free energy change (G), enthalpy change (H) and entropy change (S) were used to clarify the interaction of gas molecules with MOFs. The free energy change (G) incarnates the possibility of reaction. the standard adsorption enthalpy (ΔH^0) and entropy (ΔS^0) can be calculated from the van't Hoff equation[S13]:

$$LnK = \frac{-\Delta H}{RT} + \frac{\Delta S}{R}$$

where K is the adsorption equilibriumconstant at temperature; R is the gas constant and T is the experimental temperature. The fitted curve of ln K against 1/T is shown in Figure. S1 and figure. S2(TableS6 and TableS7). The values of ΔH and ΔS were obtained from the slope and intercept, respectively.

$$\Delta G = \Delta H - T\Delta S$$

Table S1. Van't Hoff data for the interaction of C_3H_6 with the parallel Cu-paddle wheels.

1/T	InK
0.001667	-1.6
0.002	2.1
0.0025	7.8
0.003333	17
0.005	35
0.01	92

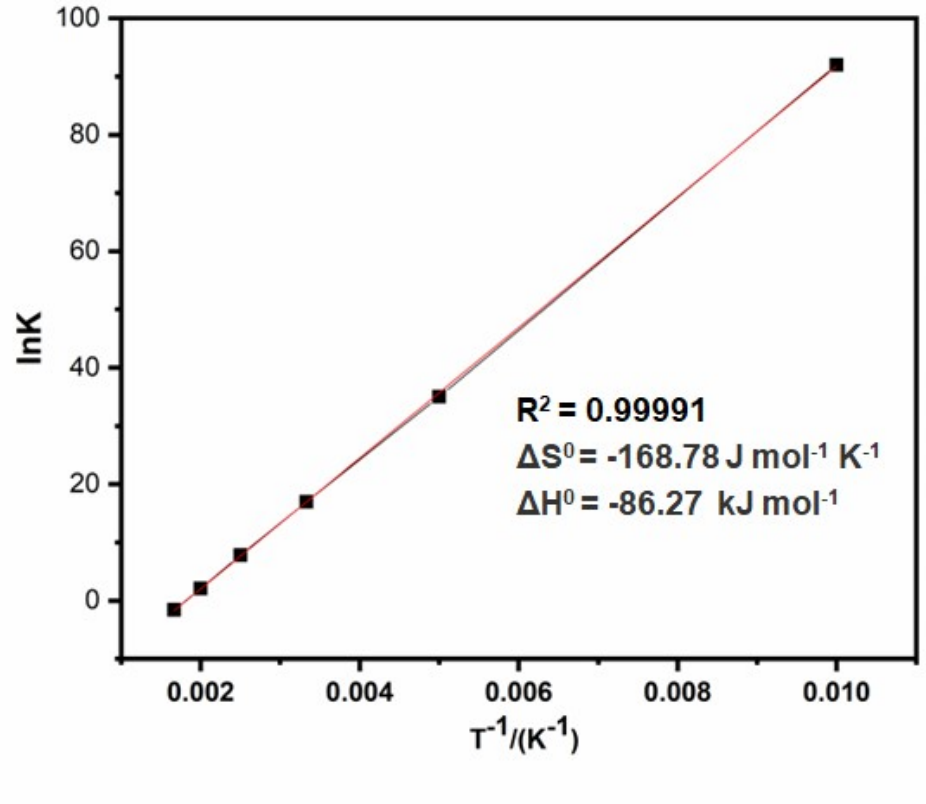

Figure S1 Van't Hoff plot for the interaction of C_3H_6 with the parallel Cu-paddle wheels (6.0 Å).

Periodic Density Functional Theory. Periodic density functional theory (DFT) calculations were performed to evaluate the adsorption energy (ΔE) for C_3H_6 and C_3H_8 adsorbed at ATC-Cu. These calculations were implemented with the Vienna ab initio Simulation Package (VASP)[S14] with the projector augmented wave (PAW)[S15] method with the Perdew-Burke-Ernzerhof (PBE) functional.[S16] Furthermore, dispersion effects were treated using the DFT-D2 correction method of Grimme.[S16] All calculations employed an energy cutoff of 600 eV. The geometric structures were fully relaxed until the forces and energy were converged to 0.01 eV $Å^{-1}$ and 10^{-5} eV, respectively. The adsorption energy (ΔE) for each site in ATC-Cu was calculated by the following:

$$\Delta E = E(\text{MOF + Adsorbate}) - E(\text{MOF}) - E(\text{Adsorbate})$$

where E (MOF + Adsorbate) is the energy of the unit cell of the MOF with the adsorbate, E(MOF) is the energy of the empty unit cell, and E(Adsorbate) is the energy of the adsorbate. The calculated ΔE values for C_3H_6 adsorbed between the two Cu^{2+} ions of neighboring copper paddle-wheel units in C_3H_6@ATC-Cu as well as C_3H_6 and C_3H_8 about such Cu^{2+} ions in the dehydrated ATC-Cu are presented in **Table S6**.

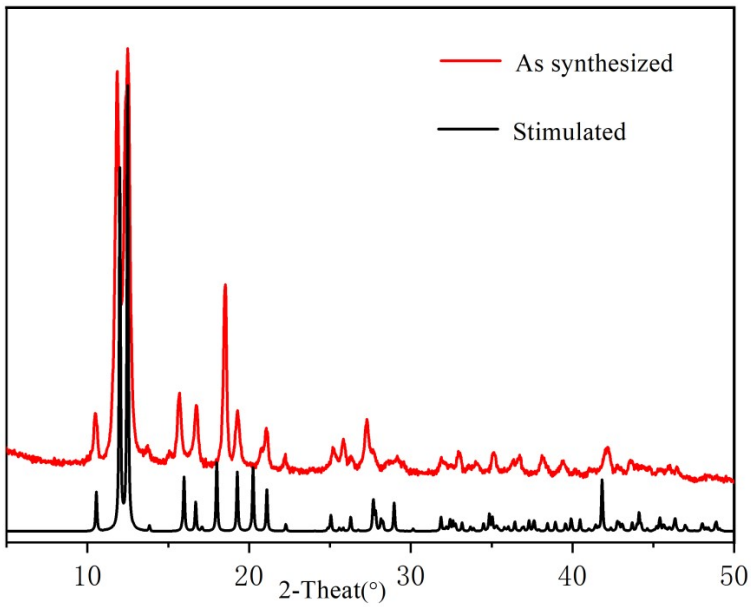

Figure S2 The calculated and synthesized PXRD patterns of $[Cu_2(ATC)(H_2O)_2]\cdot 5H_2O$.

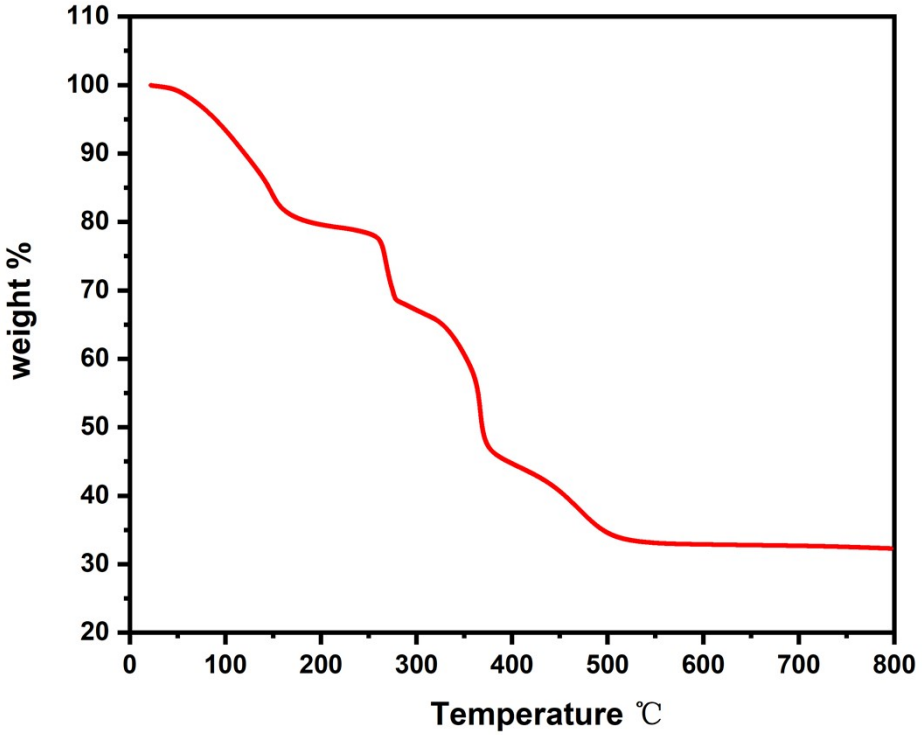

Figure S3 The TGA curve of $[Cu_2(ATC)(H_2O)_2]\cdot 5H_2O$ from room temperature to 800 °C.

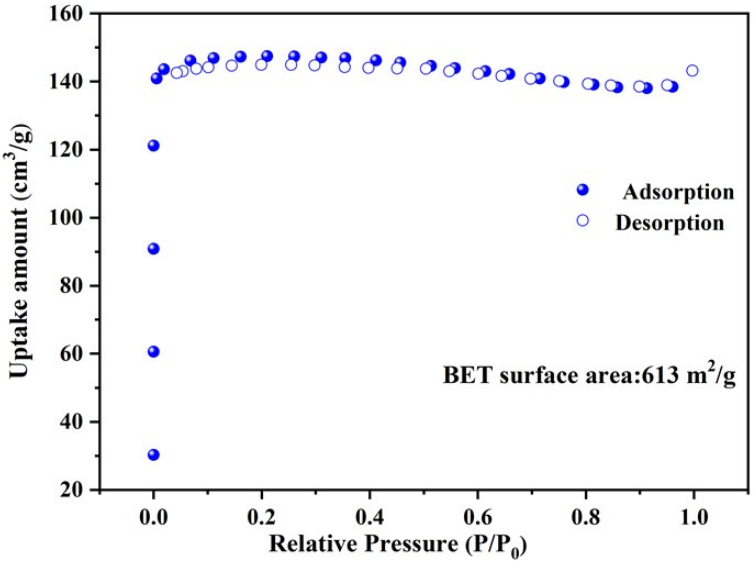

Figure S4 N_2 isotherm for ATC-Cu at 77 K.

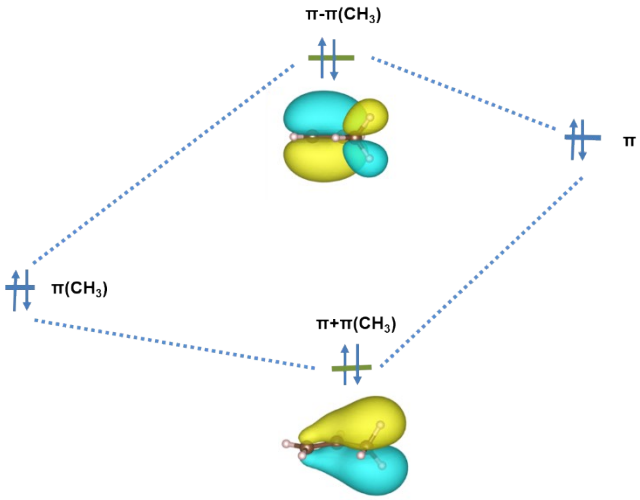

Figure S5 Molecular orbital diagram of propylene.

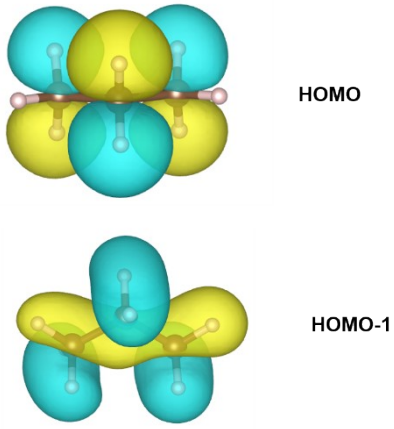

Figure S6 Molecular orbital diagram of propane.

Table S2. The binding energies of CO_2, C_3H_6 and C_3H_8.

Cluster[a]	Ead(C_3H_6)[b]	Ead(C_3H_8)[c]	ΔEad[d]
3.8	-34.59	-24.26	10.33
4	-34.79	-24.56	10.24
4.2	-35.51	-23.72	11.78
4.4	-34.51	-23.50	11.01
4.6	-86.09	-23.17	62.92
4.8	-103.08	-23.02	80.06
5	-112.95	-23.04	89.92
5.2	-116.69	-23.20	93.49
5.4	-115.62	-26.22	89.40

5.6	-111.97	-28.74	83.23
5.8	-106.58	-35.60	70.99
6	-100.33	-39.14	61.19
6.2	-94.31	-41.91	52.40
6.4	-88.99	-44.58	44.40
6.6	-84.07	-47.68	36.39
6.8	-80.24	-50.26	29.97
7	-76.88	-49.35	27.53
7.2	-74.26	-47.85	26.41
7.4	-72.52	-45.40	27.13
7.6	-72.05	-42.52	29.53
7.8	-71.03	-39.42	31.62
8	-70.24	-36.46	33.77
8.2	-69.07	-33.85	35.23
8.4	-68.26	-31.89	36.37
8.6	-66.00	-30.41	35.59
8.8	-65.20	-29.91	35.29

[a] indicates the distance between the opposite Cu paddle-wheels. [b], [c]represents the binding energy of CO_2, C_3H_6 and C_3H_8 absorbed in the cluster. [d] represents the difference between Eads (C_3H_6) and Eads (C_3H_8), all distances are expressed in Å, and all energies are expressed in kJ/mol.

Table S3. C_3H_6 and C_3H_8 uptake amount at 298K and 1 bar, and C_3H_6/C_3H_8 selectivity.

Adsorbent	Temperature (K)	IAST Selectivity	q(C_3H_8) mmol·g^{-1}	q(C_3H_6) mmol·g^{-1}	q(C_3H_6)/ q(C_3H_8)	Ref
Zn_2(5-aip)$_2$(bpy)	298	19.8	0.76	1.91	2.51	[18]
NJUBai-8	298	4	2.89	2.89	1	[19]
SIFSIX-2-Cu-i	298	4.5	1.67	2.65	1.59	[19]
GeFSIX-2-Cu-i	298	4	1.80	2.69	1.49	[19]
MOF-74-Fe	318	14.7	6.2	6.9	1.11	[20]
MOF-74-Mg	318	5.5	6	7.5	1.25	[21]
Cu@MIL-100(Fe)	323	34	2.2	3.4	1.55	[22]
TIFSIX-Cu-TPB	298	10.1	2.08	2.85	1.37	[23]
SIFSIX-Cu-TPB	298	13.8	1.46	2.45	1.68	[23]

Ni-NP	298	10.5	2.13	3.57	1.68	[24]
Mn_2(m-dobdc)	298	40	6	7.5	1.25	[25]
Fe_2(m-dobdc)	298	52	6	7.5	1.25	[25]
Co_2(m-dobdc)	298	39	6	7.5	1.25	[25]
ATC-Cu	298	58.68	3.16	3.62	1.15	This work

Table S4. C_3H_6 Q_{st} at 298 K and 100 kPa.

Adsorbent	Q_{st}（kJ/mol）	Ref
ATC-Cu	64.2	This work
$Zn_2(5\text{-aip})_2$(bpy)	46	[18]
Fe-MOF-74	44	[26]
$Cu_3(BTC)_2$	49	[27]
Mg-MOF-74	60.5	[28]
GeFSIX-2-Cu-i	36.25	[29]
SIFSIX-2-Cu-i	35.82	[29]
MIL-100（Fe）	70	[30]
TIFSIX-Cu-TPB	40.3	[23]
SIFSIX-Cu-TPB	52.5	[23]
Ni-NP	57	[24]

Table S5. The fitted parameters for the dual-site Langmuir-Freundlich equation for the single-component isotherms of C_3H_6, C_3H_8 ATC-Cu at 298 K.

	C_3H_6	C_3H_8
n_{m1}(mmol g^{-1})	2.2152759921931895	2.43301494595379
n_{m2}(mmol g^{-1})	2.1238465495419017	1.08897889579729
b_1(kPa^{-1})	0.06741850068166268	0.422031157814435
b_2(kPa^{-1})	15.179943238824258	12.829424312579
t_1	0.7455949420184158	1.807720794347285
t_2	2.777777771897063	0.7993652713416506
R^2	0.9992533504036217	0.999903307370137

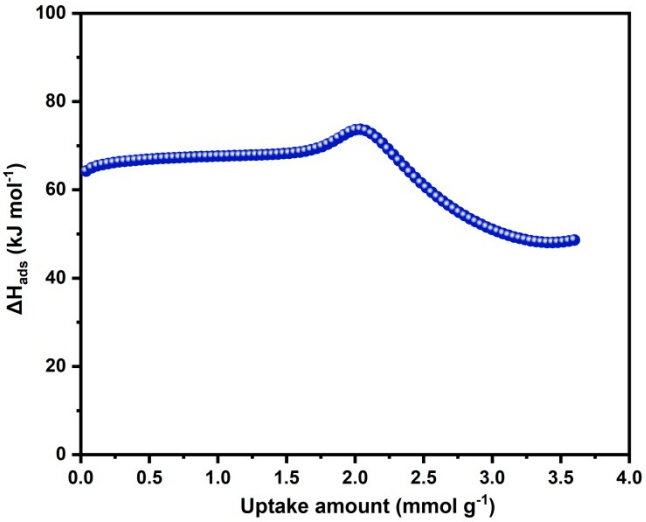

Figure S7 Adsorption enthalpies of ATC-Cu for C_3H_6.

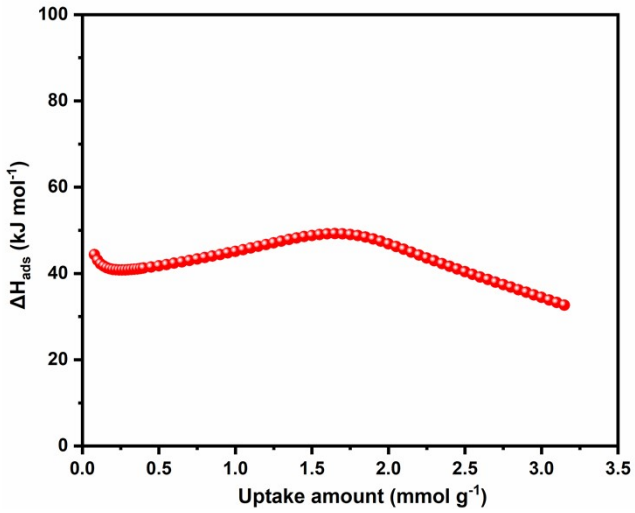

Figure S8 Adsorption enthalpies of ATC-Cu for C_3H_8.

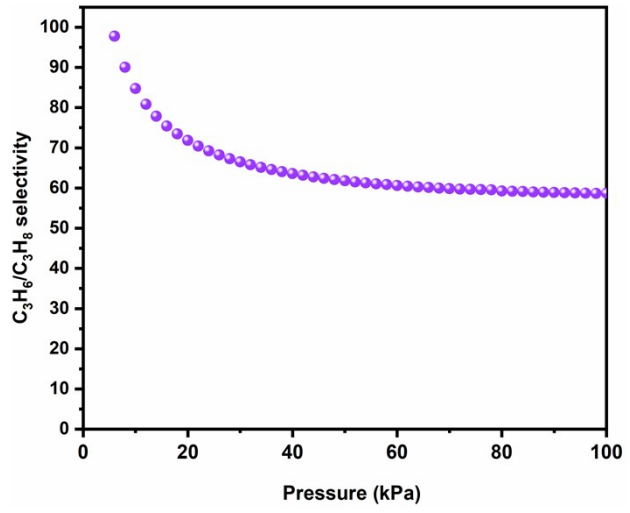

Figure S9 IAST adsorption selectivity at 298 K of ATC-Cu in C_3H_6 and C_3H_8.

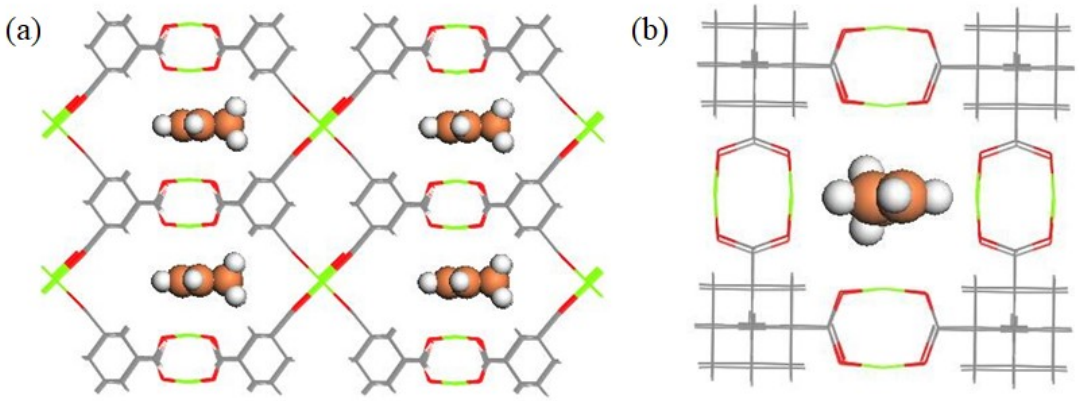

Figure S10 The DFT-optimized position of a C_3H_6 molecule in ATC-Cu.

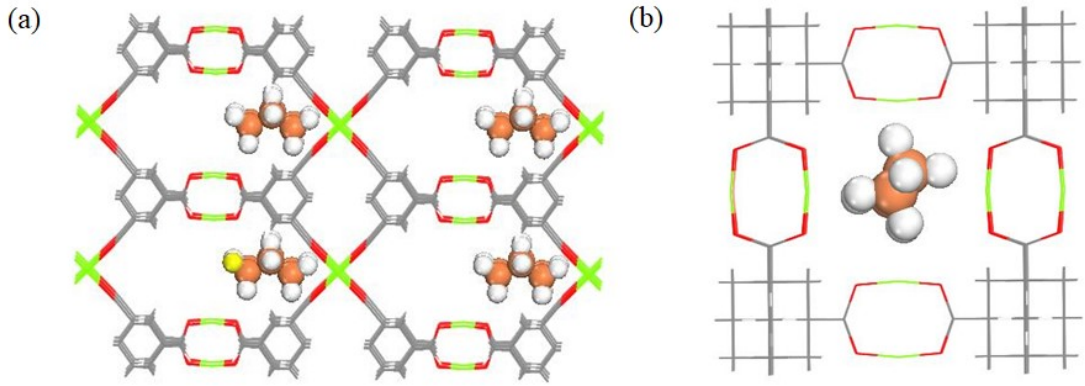

Figure S11 The DFT-optimized position of a C_3H_8 molecule in ATC-Cu.

Table S6. Calculated adsorption energies (in kJ mol^{-1}) for a single C_3H_6 molecule adsorbed between the Cu^{2+} ions of two adjacent copper paddlewheels units in the C_3H_6@ ATC-Cu, and a single C_3H_8 molecule adsorbed about this site in the latter structure (Figure S8) as determined from periodic DFT calculations using VASP.

Adsorbate	ΔE（kJ mol^{-1}）
C_3H_6(C_3H_6@ ATC-Cu)	-69.86
C_3H_8 (C_3H_8@ ATC-Cu)	-39.92

References

1 Q. Fang, S. Gu, J. Zheng, Z. Zhuang, S. Qiu and Y. Yan, *Angew. Chem. Int. Ed.* 2014, **53**, 2878-2882.

2 B. Chen, M. Eddaoudi, T. M. Reineke, J. W. Kampf, M. O'Keeffe and O. M. Yaghi, *J. Am. Chem. Soc.* 2000, **122**, 11559-11560.

3 R. T. Yang, *Gas separation by adsorption processes*, World Scientific, 1997.

4 A. L. Myers and J. M. Prausnitz, *AIChE J.* 1965, **11**, 121-127.

5 E. T. Whittaker and G. Robinson, *The calculus of observations: An introduction to numerical analysis*, Dover Publications, 1967.

6 H. Pan, J. A. Ritter and P. B. Balbuena, *Langmuir*, 1998, **14**, 6323-6327.

7 M. Frisch, G. W. Trucks, H. B. Schlegel, G. E. Scuseria, M. A. Robb, J. R. Cheeseman, G. Scalmani, V. Barone, B. Mennucci and G. Petersson, *Journal*, 2009.

8 S. Grimme, *J. Comput. Chem.* 2006, **27**, 1787-1799.

9 S. Grimme, J. Antony, S. Ehrlich and H. Krieg, *J. Chem. Phys*. 2010, **132**, 154104.

10 P. J. Hay, W. R. Wadt, L. R. Kahn and F. W. Bobrowicz, *J. Chem. Phys.* 1978, **69**, 984-997.

11 W. R. Wadt, P. J. Hay and L. R. Kahn, *J. Chem. Phys.* 1978, **68,** 1752-1759.

12 P. J. Hay and W. R. Wadt, *J. Chem. Phys.* 1985, **82**, 299-310.

13 G. Kresse and J. Hafner, *Phys. Rev. B*. 1993, **47**, 558.

14 T. Wang, Z. Zhao, L. Zhang and L. Ji, *J. Mol. Struct.*, 2009, **937**, 65-69.

15 G. Kresse and D. Joubert, *Phys. Rev. B*. 1999, **59**, 1758-1775.

16 J. P. Perdew, K. Burke and M. Ernzerhof, *Phys. Rev. Lett.* 1996, **77**, 3865.

17 S. Grimme, *J. Comput. Chem.* 2006, **27**, 1787-1799.

18 Y. Chen, H. Wu, D. Lv, N. Yuan, Q. Xia and Z. Li, *Sep. Purif. Technol.* 2018, **204**, 75-80.

19 X. Wang, P. Zhang, Z. Zhang, L. Yang, Q. Ding, X. Cui, J. Wang and H. Xing, *Ind. Eng. Chem. Res.* 2020, **59**, 3531-3537.

20 E. D. Bloch, W. L. Queen, R. Krishna, J. M. Zadrozny, C. M. Brown and J. R. Long, *Science*. 2012, **335**, 1606-1610.

21 S. J. Geier, J. A. Mason, E. D. Bloch, W. L. Queen, M. R. Hudson, C. M. Brown and J. R. Long, *Chem. Sci.* 2013, **4**, 2054-2061.

22 A. R. Kim, T.-U. Yoon, E. J. Kim, J. W. Yoon, S. Y. Kim, J. W. Yoon, Y. K. Hwang, J. S. Chang and Y. S. Bae, *Chem. Eng. J.* 2018, **331**, 777-784.

23 Y. Liu, Y. Zhang, P. Zhang, Y. Peng, X. Liu, J. Chen, S. Chen, Z. Zeng, J. Wang and S. Deng, *Chem. Eng. Process.* 2022, **172**, 108768.

24 Y. Xie, Y. Shi, H. Cui, R. B. Lin and B. Chen, *Small Struct.* 2021, **3**, 2100125.

25 J. E. Bachman, M. T. Kapelewski, D. A. Reed, M. I. Gonzalez and J. R. Long, *J. Am. Chem. Soc.* 2017, **139**, 15363-15370.

26 E. D. Bloch, W. L. Queen, R. Krishna, J. M. Zadrozny, C. M. Brown and J. R. Long, *Science*. 2012, **335**, 1606-1610.

27 J. W. Yoon, I. T. Jang, K. Y. Lee, Y. K. Hwang and J. S. J. Chang, *Bull. Korean Chem. Soc.* 2010, **31**, 220-223.

28 Z. Bao, S. Alnemrat, L. Yu, I. Vasiliev, Q. Ren, X. Lu and S. Deng, *Langmuir*. 2011, **27**, 13554-13562.

29 X. Wang, R. Krishna, L. Li, B. Wang, T. He, Y. Z. Zhang, J.-R. Li and J. Li, *Chem. Eng. J.* 2018, **346**, 489-496.

30 J. W. Yoon, Y. K. Seo, Y. K. Hwang, J. S. Chang, H. Leclerc, S. Wuttke, P. Bazin, A. Vimont, M. Daturi, E. Bloch, P. L. Llewellyn, C. Serre, P. Horcajada, J.-M. Grenèche, A. E. Rodrigues and G. Férey,*Angew. Chem., Int. Ed.* 2010, **49**, 5949-5952.